Manipulating Charges and Excitons within a Single-Host System to Accomplish Efficiency/CRI/Color-Stability Trade-off for High-Performance OWLEDs

By *Qi Wang, Junqiao Ding, Dongge Ma,* Yanxiang Cheng, Lixiang Wang,* and *Fosong Wang*

Organic white-light-emitting diode (OWLED) technology is a major focus of OLED research nowadays because of its merits of high resolution and possible flexibility for large-scale production of solid-state lighting sources and full-color OLEDs.[1,2] Recent conceptual advancements have led to many exciting approaches to high-efficiency OWLEDs, such as the combination of fluorescent/phosphorescent emitters,[3] careful management of charge distributions,[4,5] utilization of p-i-n junctions[6] through excimers[7] or mixing of excimer and exciplex emissions,[8] tandem structures,[9,10] introducing multifunctional materials,[11–16] and exciton-confining structures.[17] Nevertheless, considering future applications, further challenges are inevitably posed, that is, the requirements of very high efficiency, excellent color stability, and high color-rendering index (CRI) must be satisfied simultaneously in one device.[1,18]

In the precedent literature on OWLEDs, however, examples that can greatly resolve this issue are still rare. Although some reported OWLEDs exhibit an impressive electroluminescence (EL) efficiency, problems remain in terms of poor chromatic stability or low CRI.[4,6,15,19] Alternatively, some other OWLEDs with high color stability produce, in fact, unsatisfactory EL efficiency.[10–14] Indeed, the fact that it is hard to realize superior device efficiency/CRI/color stability trade-off forms a bottleneck to the development of OWLEDs.

In this communication, a general method to solve this trade-off problem is reported. The key features include the utilization of a single-host system, wise arrangement of the three primary-color emitters, and careful manipulation of charges and excitons. Accordingly, two types (R–G–B or RG–B, where R is red, G is green, and B is blue) of OWLEDs with superior device efficiency/CRI/color stability trade-off are demonstrated. Versatile experimental techniques are performed to access the device operational mechanism, from which we can gain a deep understanding of this novel concept and quantitatively explain why the obtained EL spectra are rather stable.

To illustrate our concept, three phosphorescent dyes, bis(2,4-diphenylquinolyl-$N,C^{2'}$)iridium(acetylacetonate) [$(PPQ)_2Ir(acac)$] for red emission,[20] *fac*-tris(2-phenylpyridine)iridium [$Ir(ppy)_3$] for green emission,[21] and iridium(III)[bis(4,6-difluorophenyl)-pyridinato-$N,C^{2'}$]picolinate (FIrpic) for blue emission, are exploited. The hole-transporting material 1,3-bis(9-carbazolyl) benzene (mCP), with a high triplet level (~2.9 eV) and wide bandgap (~3.5 eV) that can efficiently confine the triplet energy of the R, G, and B phosphors, is selected as the host material. To further confine the holes or generated excitons within the emissive region, 3-(4-biphenyl)-4-phenyl-5-(4-*tert*-butylphenyl)-1,2,4-triazole (TAZ) with a high-energy gap (~3.6 eV) is selected as the electron-transporting layer (ETL) (see Supporting Information, Fig. S1). N,N'-diphenyl-N,N'-bis(1-naphthylphenyl)-1,1′-biphenyl- 4,4′-diamine (NPB) is introduced as the hole-transporting layer (HTL).

Several strategies are employed to improve the device performance. First, we introduce a smart method that distributes different emitters in multiple regions within a single-host system in order to reduce structural heterogeneity and facilitate charge injection and transport between different emissive centers. More importantly, it allows flexible manipulation of each emissive centers as well as precious control of the exciton or charge to enhance the EL performance (see details below), which is a key difference that separates this study from the conventional single- and multi-emitting layer architectures.[3–5,11,19] Second, to ensure that the excitons formed can diffuse throughout the emissive region, we note that the phosphor with a relatively short wavelength should be placed nearest to the main recombination zone,[5] followed by the long and longer wavelength phosphors, to produce a desired output color balance. Moreover, this strategy can broaden the exciton-formation region, and thus enhance the device efficiency by lowering the local triplet accumulation.

Given these considerations, we demonstrate the first R-G-B OWLED in which the primary color emitters are separately distributed with a R–G–B sequence (see inset Fig. 1a). Remarkably, this OWLED achieves a maximum forward-viewing power efficiency (PE) and external quantum efficiency (EQE) of $\eta_p = 41.3\,\mathrm{lm\,W^{-1}}$ and $\eta_{ext} = 20.1\%$, respectively (Fig. 1a). Considering the potential for improved out-coupling, this device demonstrates the possibility of harvesting 100% excitons for

---

[*] Prof. D. G. Ma, Q. Wang, Dr. J. Q. Ding,
Prof. Y. X. Cheng, Prof. L. X. Wang, Prof. F. S. Wang
State Key Laboratory of Polymer Physics and Chemistry
Changchun Institute of Applied Chemistry
Chinese Academy of Sciences
Graduate School of the Chinese Academy of Sciences
Changchun 130022 (P. R. China)
E-mail: mdg1014@ciac.jl.cn

DOI: 10.1002/adma.200803312

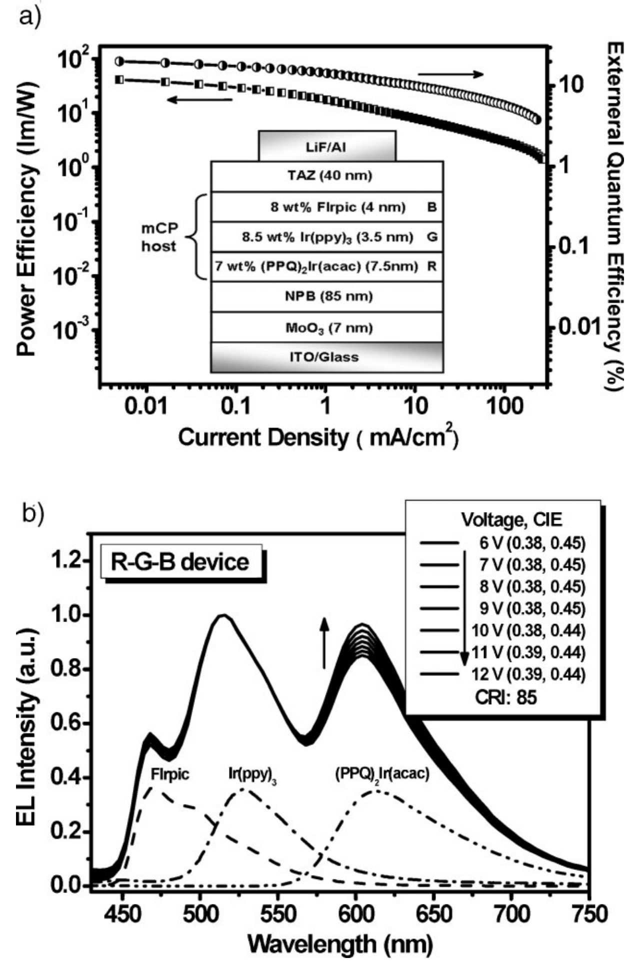

Figure 1. a) Power efficiency and EQE versus current density of a R–G–B OWLED. Inset: schematic architecture of the device. b) EL spectra of the OWLED. Dash-dot lines refer to the EL spectra of OLEDs with a single emitting layer.

white-light emission.[7,19] The device color rendition is also impressive. The EL spectrum covers all wavelengths from 450 to 750 nm (Fig. 1b), and the CRI is calculated to reach as high as 85. Notably, this OWLED possesses high color stability. When the luminance changes from 500 to 10 000 cd m^{-2} (which corresponds to an applied voltage of 6 to 12 V), the variation of the Commission Internationale de L'Eclairage (CIE) coordinates is rather small, CIE $x = 0.38$–0.39 and CIE $y = 0.45$–0.44, thus revealing superior device efficiency/CRI/chromatic-stability trade-off.

To further show the merit of this device, we compare the EQE of the OWLED with that of three monochromatic devices using the same material combinations (Supporting Information Fig. S2). The maximum EQEs obtained of the R, G, and B devices are 6.0, 10.8, and 13.3%, respectively, which are much lower than that of the white device (20.1%). This strongly proves that the formed excitons are distributed in multiple regions,[22] and that the energy loss associated with the triplet or charge-carrier leakage is negligible in this OWLED.[3]

In the R–G–B OWLED, however, we note a small color shift associated with the intense charge-trapping effect of the heavily doped (7 wt%) R species with increasing voltage.[5] To produce further improvement, we propose the second RG–B OWLED, where R- and G-light emitters are combined into one region (see inset Fig. 2a). As expected, the device efficiency is still maintained at a high level, that is, the maximum forward-viewing PE and EQE are $\eta_{\mathrm{p}} = 37.3\ \mathrm{lm\,W^{-1}}$ and $\eta_{\mathrm{ext}} = 19.1\%$ (Fig. 2a). Surprisingly, the obtained EL spectrum turns out to be rather stable (Fig. 2b). In a wide range of operational voltages, the CIE coordinates of (0.39,0.42) are constant, and the CRIs remain at 80. To our knowledge, this is one of the best results obtained, considering both efficiency and color-rendition issues.

To demonstrate the emission mechanism in the RG–B OWLED, the excitation spectra and photoluminescence (PL) transient characteristics in different cases of organic films (film 1–4, see the upper part of Fig. 3) were obtained.[16,19,23] Figure 3a displays the excitation spectra of film 4 composed of mCP: Ir(ppy)$_3$: (PPQ)$_2$Ir(acac)/mCP: FIrpic by monitoring at $\lambda = 470$ nm to examine FIrpic, 517 nm for Ir(ppy)$_3$, and 604 nm for (PPQ)$_2$Ir(acac).[23] The excitation spectrum of a pure mCP film is also displayed.[16] As shown, the excitation spectra of FIrpic and Ir(ppy)$_3$ are nearly the same, indicating that the FIrpic–Ir(ppy)$_3$ energy transfer is quite efficient. In addition, as previously established, the mCP–FIrpic energy transfer is extremely facile and complete.[16] Combining

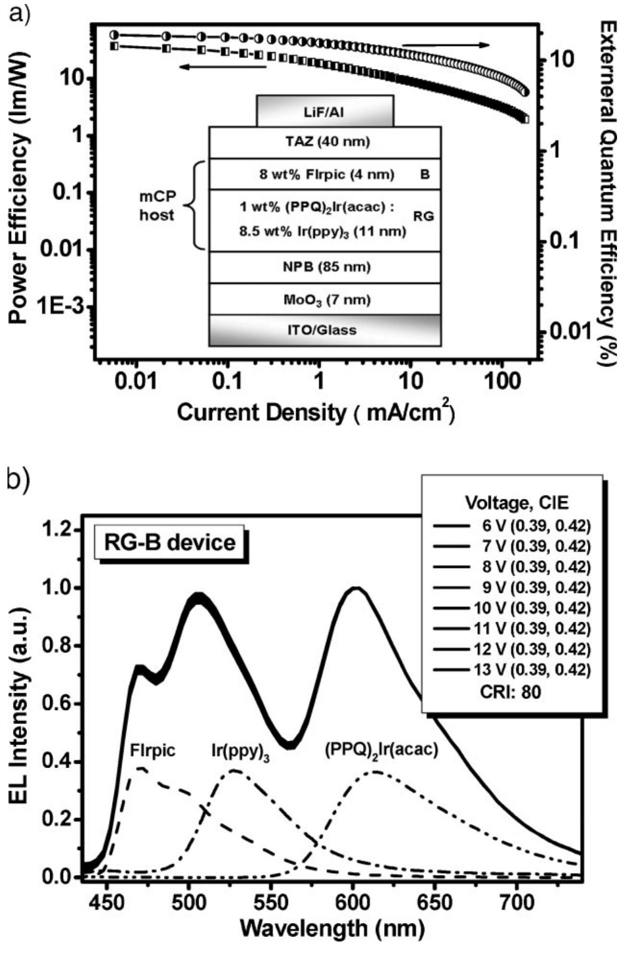

Figure 2. a) Power efficiency and EQE versus current density of a RG–B OWLED. Inset: schematic structure of the device. b) EL spectra of the OWLED.

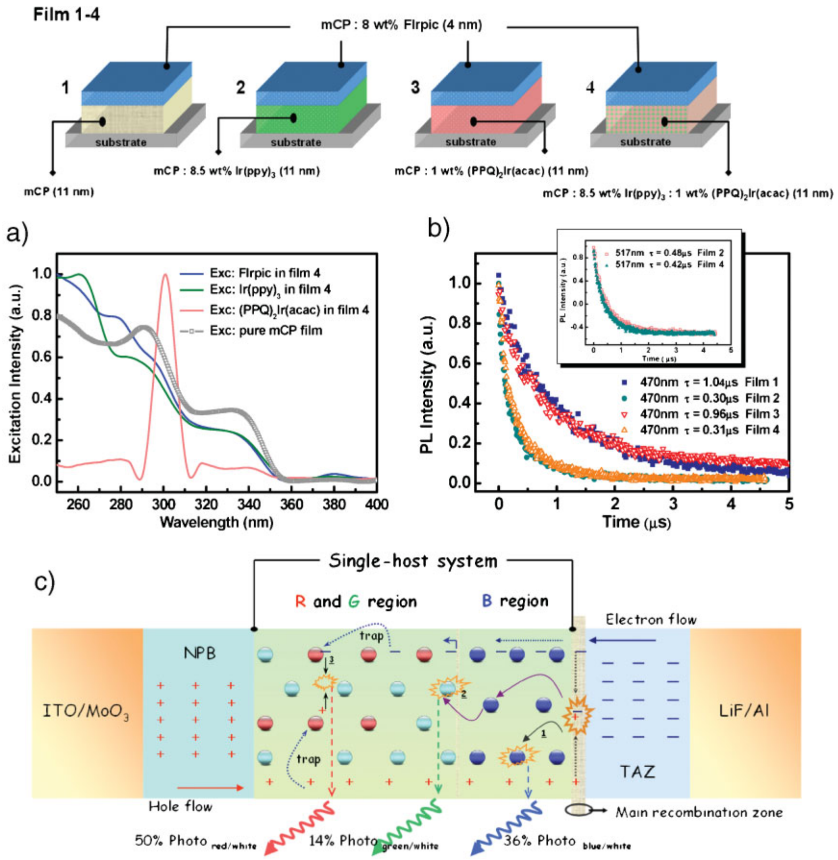

Figure 3. Upper: Structures of the four tested films (Film 1–4). a) Excitation spectra of FIrpic, $Ir(ppy)_3$, and $(PPQ)_2Ir(acac)$ in film 4, and pure mCP. b) Decay transients of FIrpic in film 1–4. Inset: PL decay transients of $Ir(ppy)_3$ in film 2 and 4. Note that the PL decays of the phosphors are taken from their respective peak emissions, and lifetimes are estimated from monoexponential fits to the experimental data. c) Proposed operational principle of the RG-B OWLED. The energy transfer from mCP to FIrpic (●) ensures blue-light emission (1). The sequential mCP–FIrpic–$Ir(ppy)_3$ (●) energy transfer dominates green-light emission (2), while direct recombination of the electrons and the trapped holes on $(PPQ)_2Ir(acac)$ (●) sites guarantees red-light emission (3).

the above results and the fact that the main recombination zone of the free electrons and holes is situated close to the mCP/TAZ interface, $Ir(ppy)_3$ emission is mainly attributed to the sequential mCP–FIrpic–$Ir(ppy)_3$ energy transfer in the RG–B device.[19] Here, we note that the self-charge-trapping effect barely contributes to the green emission (discussed in detail below). Alternatively, the distinct excitation spectrum of $(PPQ)_2Ir(acac)$ indicates that the red emission cannot be associated with the energy transfer from mCP, FIrpic, or $Ir(ppy)_3$, which is presumably a consequence of the rather low doping concentration of $(PPQ)_2Ir(acac)$, which causes the lumophores to lie beyond the effective Dexter-transfer radius of excited molecules.[5,16,19]

The transient PL decay of FIrpic (recorded at 470 nm) in films 1–4 (see Fig. 3b) can provide further information. The lifetime of FIrpic decreases from $\tau = 1.04\,\mu s$ in film 1 to $\tau = 0.30\,\mu s$ in film 2. This suggests that FIrpic emission is quenched primarily by energy transfer to $Ir(ppy)_3$,[19] and provides strong proof that $Ir(ppy)_3$ emission is dominated by the mCP–FIrpic–$Ir(ppy)_3$ energy transfer in EL. However, the nearly unchanged lifetimes of FIrpic in film 1 ($\tau = 1.04\,\mu s$) and 3 ($\tau = 0.96\,\mu s$) indicate the insignificant energy transfer from FIrpic to $(PPQ)_2Ir(acac)$. In addition, FIrpic exhibits almost the same lifetime in film 2 ($\tau = 0.30\,\mu s$) and 4 ($\tau = 0.31\,\mu s$), which further justifies the two points above. As calculated, the $Ir(ppy)_3$ lifetime (recorded at 517 nm) in films 2 and 4 remains unchanged (see inset in Fig. 3b), suggesting that energy transfer from $Ir(ppy)_3$ to $(PPQ)_2Ir(acac)$ is also negligible.[5] Therefore, we conclude that a self-charge-trapping effect dominates the $(PPQ)_2Ir(acac)$ emission in the RG–B OWLED.

Based on this working model, the fraction of excitons directly trapped by $(PPQ)_2Ir(acac)$ has been calculated to be $\chi^{R}_{\mathrm{Trap,\ RG-B}} = (52 \pm 2)\,\%$ during the entire EL process (see Experimental section). Furthermore, by fitting the white-light spectrum, it was found that 50% of the total emission originates from $(PPQ)_2Ir(acac)$. Combining both results, it is once again confirmed that direct carrier trapping indeed dominates the red-light emission, and a self-charge-trapping effect barely contributes to the green-light emission in the RG–B device. Accordingly, we calculate that approximately 14% of the total excitons are energy transferred to $Ir(ppy)_3$ for green-light emission, whereas 36% are transferred for blue-light emission. This technique is similar to those discussed previously by Sun et al.[3]

In fact, we note that FIrpic is essential in controlling the color rendition. As is known, FIrpic exhibits bipolar transport characteristics and related higher electron mobility ($\sim 10^{-6}\,\mathrm{cm^2\,v^{-1}\,s^{-1}}$).[24] Here, electron- and hole-only devices based on pure FIrpic are fabricated, and it is shown that the electron current is approximately one order of magnitude larger than the hole current during the whole process (Supporting Information, Fig. S3). As such, the electrons and holes injected can balance well in this hole-type system by doping of the ambipolar species, which results in improvement of the recombination efficiency.[19,25] More importantly, it allows resonant electron diffusion into $(PPQ)_2Ir(acac)$ sites (given the nearly aligned lowest unoccupied molecular orbital (LUMO) levels between them, see Fig. S1 in the Supporting Information) and persistent exciton diffusion (~14% green/total) into $Ir(ppy)_3$ molecules, and meanwhile ensures that the fraction of electrons/excitons directly trapped by $(PPQ)_2Ir(acac)$ is constant (~50%) during the entire EL process, leading to superior color balance along with chromatic stability (Fig. 2b). Furthermore, this unique working model broadens the exciton formation region, thus greatly enhancing device efficiency by reducing exciton/charge accumulation.[22] Apparently, careful manipulation of charges and excitons is the key point to realizing such high performance in this single-host system. The principle of the RG–B device operation is illustrated in Figure 3c.

Table 1. A summary of device characteristics.

Architecture	Hole injection layer	η_{ext} [%]	η_p [lm W^{-1}]	CIE	ΔCIE [a] (Δx, Δy)	CRI
R-G-B type [b]	MoO_3	20.1	41.3	(0.38, 0.45)	(+0.01, −0.01)	85
R-G-B type	PEDOT:PSS	18.5	35.0	(0.35, 0.42)	(0.00, −0.01)	88
RG-B type	MoO_3	19.1	37.3	(0.39, 0.42)	(0.00, 0.00)	80
RG-B type	PEDOT:PSS	16.1	30.2	(0.36, 0.38)	(0.00, 0.00)	80
R'G'-B type [c]	MoO_3	17.6	32.4	(0.35, 0.44)	(±0.01, −0.01)	83
R'G'-B type	PEDOT:PSS	18.4	33.9	(0.42, 0.42)	(0.00, 0.00)	75

[a] ΔCIE: CIE variations ranging from 500 to 10 000 cd m^{-2}. [b] R–G–B type refers to R–G–B structure, while RG–B type refers to RG-B architecture described in the text. [c] 'G' means the green phosphor is $(ppy)_2Ir(acac)$ instead of $Ir(ppy)_3$ (G). Details are available in the Supporting Information, Fig. S6.

In the R–G–B device, however, the energy transfer from $Ir(ppy)_3$ to $(PPQ)_2Ir(acac)$ cannot be neglected, because of the high doping concentration of the latter (see PL lifetime experiments in Supporting Information, Fig. S4). In addition, besides the FIrpic–$Ir(ppy)_3$ energy-transfer process, we find that direct carrier trapping in $Ir(ppy)_3$ sites also contributes to green-light emission. Herein, we give the fraction of excitons directly trapped by, and formed on, both R and G species by $\chi^{\text{R and G}}_{\text{Trap, R-G-B}} = 69 \pm 2\ \%$ (see Experimental section), which is nearly constant during the whole process. This explains quantitatively why the EL spectrum is so stable in the R–G–B OWLED (Fig. 1b). Furthermore, by fitting the white-light spectrum, it was found that 46% of the total emission originates from the $(PPQ)_2Ir(acac)$ (compare $\chi^{\text{R and G}}_{\text{Trap, R-G-B}} = (69 \pm 2)\%$).[3] This strongly proves that a self-charge-trapping effect also contributes to green-light emission in the R–G–B device. FIrpic is, as previously mentioned, essential for control of the color rendition. Here, a R–G control device is fabricated with the same structure as the R–G–B OWLED but with no FIrpic doping in the B layer (Supporting Information, Fig. S5). The large variation of the CIE coordinates ($\Delta x \sim 0.08$, $\Delta y \sim 0.07$) of the R–G control device relative to that of the R–G–B white-light device ($\Delta x \sim 0.01$, $\Delta y \sim 0.01$) clearly proves this point.

Remarkably, according to our concept, a series of OWLEDs with extremely high EL performances have subsequently been demonstrated by incorporating either a new G species, bis(2-phenylpyridine)iridium(III) acetylacetonate [$(ppy)_2Ir(acac)$],[26] or another hole-injection material, poly(3,4-ethylenedioxythiophene) poly(styrene sulfonate) (PEDOT:PSS, see Table 1). Encouraged by these impressive results, our design concept can be a universal method for achieving high-performance OWLEDs.

We note that our devices can indeed harvest nearly all the generated excitons at low currents. However, like most conventional all-phosphor OWLEDs,[16,19] the notorious efficiency roll-off problem (the EQE of the RG–B device decreases to 13.6% at 1000 cd m^{-2}) still remains, because of the stronger dissociation and annihilation of excitons on charge carriers at higher currents that have been well established by Kalinowski et al.[27] To fully exploit the potential of our concept, the introduction of a novel ambipolar host material with high mobility and high triplet level would be more helpful, solving the roll-off problem and thus revealing an even more superior efficiency/reduced efficiency roll-off/color rendition trade-off necessary for lighting applications.[3,8,17,27]

In conclusion, the present study reports on a general method to significantly boost the performance of OWLEDs by exploiting a single-host system where the three primary color emitters are rationally arranged. Accordingly, a series of OWLEDs with superior device efficiency/CRI/color stability trade-off are demonstrated. Comprehensive experimental and theoretical evidence show that the careful manipulation of charges and excitons is the key point to realizing such high performance. We believe that this simple design concept can provide a new avenue for achieving ultrahigh-performance OWLEDs.

Experimental

Device Fabrication and Testing: Devices were grown on glass substrates precoated with an indium tin oxide (ITO) layer 180 nm thick that had a sheet resistance of 10 Ω square^{-1}. The substrates were thoroughly cleaned before use. All layers were grown in succession by thermal evaporation without breaking vacuum ($\sim 5 \times 10^{-4}$ Pa). Current–brightness–voltage characteristics were measured by using a Keithley source measurement unit (Keithley 2400 and Keithley 2000) with a calibrated silicon photodiode. The EL spectra were measured using a spectrascan PR650 spectrophotometer. All the measurements were carried out in ambient atmosphere.

Measurements of Photophysical Properties: Excitation spectra were measured using a Perkin–Elmer LS 50B spectrofluorometer. PL transient measurements were performed at 300 K, using a Quanty-ray DCR-2 pulsed Nd:YAG laser with a THG 355 nm output and ~3 ns pulse width.

Data Analysis: RG–B type: Given the distinct emission nature of each dopant, the OWLED EQE $\eta_{\text{ext, RG-B}}$ was simply described as:

$$\eta_{\text{ext, RG-B}} = \eta_{\text{B}}\left(1 - \chi^{\text{R}}_{\text{Trap, RG-B}}\right) + \eta_{\text{RG}} \tag{1}$$

where η_B is the EQE of a purely FIrpic-doped device, η_{RG} is the sum of the quantum efficiency that originated from red- and green-light emission in the RG–B device, and $\chi^{\text{R}}_{\text{Trap, RG-B}}$ is the fraction of excitons directly trapped by $(PPQ)_2Ir(acac)$. By fitting the OWLED spectrum (Fig. 2b) to the EL spectra of the three individual dopant materials, and considering the photon energy in these power spectra, it was found that 36% of the total quantum efficiency was a result of the emission from FIrpic, while 50% is from $(PPQ)_2Ir(acac)$. Given the performance characteristics (η_B) of the purely FIrpic-doped device, we calculated $\chi^{\text{R}}_{\text{Trap, RG-B}} = (52 \pm 2)\ \%$ from the first term in Equation 1.[3]

R–G–B type: The EQE $\eta_{\text{ext, R-G-B}}$ of the R–G–B device can be expressed by:

$$\eta_{\text{ext, R-G-B}} = \eta_{\text{B}}\left(1 - \chi^{\text{R and G}}_{\text{Trap, R-G-B}}\right) + \eta_{\text{R-G}} \tag{2}$$

where $\eta_{\text{R-G}}$ is the sum of the quantum efficiency that originated from the red and green emissions in the R–G–B device. $\chi^{\text{R and G}}_{\text{Trap, RG-B}}$ depicts the fraction of excitons trapped by $(PPQ)_2Ir$ (acac) and $Ir(ppy)_3$ together. By fitting the

OWLED spectrum (Fig. 1b), it was found that 24% of the total quantum efficiency was a result of the emission from FIrpic, while 46% was from $(PPQ)_2Ir(acac)$. Accordingly, we obtained $\chi^{\mathrm{R\ and\ G}}_{\mathrm{Trap,\ R-G-B}} = (69\pm\ 2)\,\%$ from the first term in Equation 2.

Acknowledgements

The authors thank the Hundreds Talents program of Chinese Academy of Sciences, the National Science Fund for Distinguished Young Scholars of China (50325312), the Foundation of Jilin Research Council (20050517, 20080337), Foundation of Changchun Research Council (2007GH06), Science Fund for Creative Research Groups of NSFC (20621401) and Ministry of Science and Technology of China (863 program No. 2006AA03A161, 973 program No. 2009CB930603) for the support of this research. Supporting information for this article is available online at Wiley InterScience or from the authors.

Received: November 11, 2008
Revised: January 10, 2009
Published online:

[1] F. So, J. Kido, P. Burrows, *MRS Bull.* **2008**, *33*, 663.
[2] B. W. D'Andrade, *Nat. Photon.* **2007**, *1*, 33.
[3] Y. Sun, N. C. Giebink, H. Kanno, B. Ma, M. E. Thompson, S. R. Forrest, *Nature* **2006**, *440*, 908.
[4] J. Huang, G. Li, E. Wu, Q. Xu, Y. Yang, *Adv. Mater.* **2006**, *18*, 114.
[5] B. W. D'Andrade, M. E. Thompson, S. R. Forrest, *Adv. Mater.* **2002**, *14*, 147.
[6] G. Schwartz, M. Pfeiffer, S. Reineke, K. Walzer, K. Leo, *Adv. Mater.* **2007**, *19*, 3672.
[7] E. L. Williams, K. Haavisto, J. Li, G. E. Jabbour, *Adv. Mater.* **2007**, *19*, 197.
[8] J. Kalinowski, M. Cocchi, D. Virgili, V. Fattori, J. A. G. Williams, *Adv. Mater.* **2007**, *19*, 4000.
[9] C.-C. Chang, J.-F. Chen, S.-W. Hwang, C. H. Chen, *Appl. Phys. Lett.* **2005**, *87*, 253501.
[10] F. W. Guo, D. G. Ma, *Appl. Phys. Lett.* **2005**, *87*, 173510.
[11] Y.-S. Park, J.-W. Kang, D. M. Kang, J.-W. Park, Y.-H. Kim, S.-K. Kwon, S. C. Shin, J.-J. Kim, *Adv. Mater.* **2008**, *20*, 1957.
[12] T.-H. Kim, H. K. Lee, O. O. Park, B. D. Chin, S.-H. Lee, J. K. Kim, *Adv. Funct. Mater.* **2006**, *6*, 611.
[13] C.-L. Ho, W.-Y. Wong, Q. Wang, D. G. Ma, L. X. Wang, Z. Y. Lin, *Adv. Funct. Mater.* **2008**, *18*, 928.
[14] P.-I. Shih, C.-F. Shu, Y.-L. Tung, Y. Chi, *Appl. Phys. Lett.* **2006**, *88*, 251110.
[15] B. P. Yan, Cecil, C. C. Cheung, S. C. F. Kui, H. F. Xiang, V. A. L. Roy, S. J. Xu, C. M. Che, *Adv. Mater.* **2007**, *19*, 3599.
[16] Q. Wang, J. Q. Ding, D. G. Ma, Y. X. Cheng, L. X. Wang, X. B. Jing, F. S. Wang, *Adv. Funct. Mater.* **2009**, *19*, 84.
[17] S.-J. Su, E. Gonmori, H. Sasabe, J. Kido, *Adv. Mater.* **2008**, *20*, 4189.
[18] M. C. Gather, R. Alle, H. Becker, K. Meerholz, *Adv. Mater.* **2007**, *19*, 4460.
[19] B. W. D'Andrade, R. J. Holmes, S. R. Forrest, *Adv. Mater.* **2004**, *16*, 624.
[20] J. Q. Ding, J. Gao, Q. Fu, Y. X. Cheng, D. G. Ma, L. X. Wang, *Synth. Met.* **2005**, *155*, 539.
[21] M. A. Baldo, S. Lamansky, P. E. Burrows, M. E. Thompson, S. R. Forrest, *Appl. Phys. Lett.* **1999**, *75*, 4.
[22] Y. Sun, S. R. Forrest, *Appl. Phys. Lett.* **2007**, *91*, 263503.
[23] J.-J. Lin, W.-S. Liao, H.-J. Huang, F.-I. Wu, C.-H. Cheng, *Adv. Funct. Mater.* **2008**, *18*, 485.
[24] N. Matsusue, Y. Suzuki, H. Naito, *Jpn. J. Appl. Phys.* **2005**, *44*, 3691.
[25] T. Tsuzuki, S. Tokito, *Adv. Mater.* **2007**, *19*, 276.
[26] C. Adachi, M. A. Baldo, M. E. Thompson, S. R. Forrest, *J. Appl. Phys.* **2001**, *90*, 5048.
[27] a) J. Kalinowski, W. Stampor, J. Mężyk, M. Cocchi, D. Virgili, V. Fattori, P. Di Marco, *Phys. Rev. B* **2002**, *66*, 235321. b) J. Kalinowski, W. Stampor, J. Szmytkowski, D. Virgili, M. Cocchi, V. Fattori, C. Sabatini, *Phys. Rev. B* **2006**, *74*, 085316.